Midlatitude North Atlantic heat transport: A time series based on satellite and drifter data

Will R. Hobbs[1] and Joshua K. Willis[1]

Received 3 February 2011; revised 19 October 2011; accepted 6 November 2011; published 11 January 2012.

[1] Using temperature, salinity, and displacement data from Argo floats combined with satellite sea surface height, a time series of the Atlantic meridional heat transport from January 2002 to August 2010 has been estimated for 41°N. The calculation method is validated against hydrographic climatologies and output from the ECCO2 ocean data assimilation model, and the assumptions are shown to be reasonable; the greatest source of error is from the sparse distribution of Argo floats. The mean heat transport is 0.50 ± 0.1 PW, which is consistent with previous estimates made using surface flux data but is low compared estimates from hydrographic cruise data. Consistent with results from the RAPID array, the heat transport has a significant annual cycle and high degree of subannual variability, indicating that statistical uncertainty in previous calculations may have been underestimated. There is little evidence of a trend over the short period of available data. Correlations with sea surface temperature suggest clear physical relationships between heat transport and SST, even on the short time scales of available data.

Citation: Hobbs, W. R., and J. K. Willis (2012), Midlatitude North Atlantic heat transport: A time series based on satellite and drifter data, *J. Geophys. Res.*, *117*, C01008, doi:10.1029/2011JC007039.

1. Introduction

[2] The Atlantic Meridional Overturning Circulation (AMOC) is characterized by a relatively warm northward flow above an approximate depth of 1000 m, and a relatively cold southward return flow. As such, it is responsible for a net heat transport into the North Atlantic, which is thought to have important climatic consequences at multidecadal timescales [*Delworth and Mann*, 2000; *Knight et al.*, 2005; *Zhang et al.*, 2010]. *Knight et al.* [2005] link variations of the AMOC to the Atlantic Multidecadal Oscillation [*Kerr*, 2000], a pattern of North Atlantic sea surface temperature variability that has been implicated in hurricane variability [*Goldenberg et al.*, 2001], rainfall in the African Sahel and in Northeast Brazil [*Folland et al.*, 1986; *Rowell et al.*, 1995; *Folland et al.*, 2001], Alpine glacier mass balance [*Huss et al.*, 2010], and with North American climate [*Sutton and Hodson*, 2005].

[3] Model simulations consistently predict a slow down of the AMOC in response to anthropogenic climate change, due to increased freshwater flux from the melting Greenland ice sheet, and changes in high latitude surface heat fluxes [e.g., *Gregory et al.*, 2005; *Weaver et al.*, 2007]. The magnitude of the AMOC slow down is highly uncertain, however, with reductions in response to a 1%/year increase in atmospheric CO_2 in the range of 10–50% simulated by global climate models used in the IPCC Fourth Assessment Report [*Gregory et al.*, 2005]. Related to this is the great uncertainty in the observed Atlantic meridional heat transport (MHT). Table 1 shows previous estimates of 36–55°N Atlantic MHT arranged by latitude. Even accounting for the reduction in mean MHT with latitude north of 26°N [*Trenberth and Caron*, 2001; *Ganauchad and Wunsch*, 2003] there is a wide range of estimates from 0.3 to 1.1 PW. Of the studies in Table 1 that estimated changes over time, there is general agreement of an increase in heat transport from the late 1950s to the 1990s, with a possible decrease over the 1990s. However, with the exception of studies based on atmospheric or ocean reanalysis, these estimates are largely made by inverse box models based on few, nearly synoptic observations, and may be sensitive to aliasing due short-term and seasonal variability [*Cunningham et al.*, 2007].

[4] Given the AMOC's potential importance for the Northern Hemisphere climate system, and the great uncertainty regarding its response to anthropogenic climate change, there is a clear and pressing need for reliable, continuous observations of North Atlantic heat transport. The RAPID array, which has been deployed at 26.5°N since 2004, is a network of moorings capable of providing the first such measurements, and has been used to estimate Atlantic heat transport [*Johns et al.*, 2011]. However, it is not well known how the variability at the RAPID array's latitude represents the variability at mid latitudes. Recent work suggests that the AMOC's modes of variability are quite different between low and mid latitudes on interannual timescales [*Bingham et al.*, 2007; *Zhang*, 2010], and even on decadal timescales [*Lozier et al.*, 2010], which challenges

[1]NASA Jet Propulsion Laboratory, California Institute of Technology, Pasadena, California, USA.

0148-0227/12/2011JC007039

Table 1. Previous Estimates of Atlantic Meridional Heat Transport by Latitude[a]

	Data Source	Mean MHT (PW)	Latitude (°N)	41°N/NOC Flux (PW)
Roemmich and Wunsch [1985]	CTD sections (Jun 1981)	0.8	36	0.69
Rintoul and Wunsch [1991]	CTD sections (Jun 1981)	1.3 ± 0.02		
Koltermann et al. [1999]	CTD sections (Apr 1959, Jun 1981, Sep 1993)	0.47 ± 0.24		
		1.29 ± 0.17		
		0.70 ± 0.15		
Sato and Rossby [2000]	WOA09 1994	1.2 ± 0.3		
Talley [2003]	CTD section (Jun 1981)	0.86 ± 0.1–0.2		
McDonagh et al. [2010]	CTD section (May 2005)	1.14 ± 0.12		
Hsiung [1985]	in situ surface fluxes (1946–1979)	0.64 (no error estimate)	40	0.54
Trenberth and Caron [2001]	atmospheric reanalysis radiative flux (1985–1989)	0.6 ± 0.1 (ERA15)		
		0.5 ± 0.08 (NCEP)		
Zheng and Giese [2009]	SODA reanalysis (1958–2004)	1.09 (0.12)		
Talley [2003]	CTD section (Apr 1957)	0.62 ± 0.1–0.2	45	0.42
Ganachaud and Wunsch [2003]	CTD section (Jul 1993)	0.6 ± 0.09	47	0.40
Koltermann et al. [1999]	CTD sections (Apr 1957, Apr 1982, Jul 1993)	0.27 ± 0.15	48	0.39
		0.62 ± 0.11		
		0.53 ± 0.12		
Lumpkin et al. [2008]	CTD sections (Jul 1993, May 1996, Jun 1997, May 1998, May 2000)	0.53 ± 0.1		
Hsiung [1985]	in situ surface fluxes (1946–1979)	0.45 (no error estimate)	50	0.36
Zheng and Giese [2009]	SODA reanalysis (1958–2004)	0.71 (0.05)		
Bacon [1997]	CTD section (Aug 1991)	0.28 ± 0.06	~55	0.29

[a]Second column shows data source (and where appropriate, hydrographic cruise date); third column shows mean values (including error bars where given, or standard deviation in parentheses); fourth column shows latitude; rightmost column shows an estimate for each latitude based on the Argo/SSH 41°N, and net surface heat flux integrated from 41°N to appropriate latitude, using the climatology of *Grist and Josey* [2003].

the paradigm of a meridionally coherent AMOC. In this study, we extend previous work [*Willis and Fu*, 2008; *Willis*, 2010] to estimate the net heat transport integrated across 41°N, using hydrographic and drift data from Argo floats, combined with satellite altimetry and scatterometry. The mean heat transport is compared with climatological estimates for the same latitude, and the variability is compared with data over the same period from the RAPID array, and ocean synthesis data from the Estimating the Circulation and Climate of the Ocean, Phase II (ECCO2) product [*Menemenlis et al.*, 2005a, 2005b].

2. Method

[5] The primary data were temperature and salinity observations recorded by the Argo float network (http://www.argo.ucsd.edu/). These floats drift for a specified time period at a preset depth (typically ~10 days at 1000 m), before sinking to 2000 m and recording temperature/salinity profiles to the surface; at the surface the data is uploaded to satellite along with the float's current location. This results in frequent, global records of temperature and salinity to 2000 m as well as a displacement, from which the velocity at the drift depth can be calculated. Argo data have been previously used in inverse box model estimates of North Atlantic meridional overturning [*Hernández-Guerra et al.*, 2010], but in that study the Argo data were time-averaged and the temporal variability could not be represented. In this work, we compute four-dimensional velocity and state estimates from time-varying fields of temperature, salinity and density, and the 1000 dbar reference velocity computed from Argo and satellite altimeter sea surface height (SSH) data from the AVISO DT-MSLA product (www.aviso.oceanobs.com). Here we give a brief outline of this method; for a more complete description the reader is referred to *Willis and Fu* [2008].

[6] The estimate for a 3-month average density field ($\rho_{estimate}$) can be summarized as

$$\rho_{estimate} = \left\{ \rho_{profile} - \alpha \times SSH \right\} + \overline{\alpha \times SSS} \qquad (1)$$

where SSH is the satellite sea surface height anomaly, $\rho_{profile}$ is the density profile from Argo data, α is a depth and location dependent regression coefficient between SSH and $\rho_{profile}$, and an overbar represents a 3-month mean and curly brackets denote an objectively mapped field. To calculate the regression coefficient (α in equation (1)) the anomaly profiles were grouped into 4° longitude × 2° latitude × 10 dbar depth bins and regressed against the SSH anomaly at each profile's time and location; this gave a statistical relationship between SSH and the subsurface state variables for each bin. Next, the SSH data alone were used to generate "first guess" maps of subsurface salinity, temperature and density from the regression coefficients for each 10-day AVISO data period; this is the second term in the curly brackets in equation (1). The difference between each Argo profile and the first-guess maps were then objectively mapped onto a 1/4° latitude × 1/4° longitude × 10 m depth grid for all 3-month periods from 2002 to 2010, and the resulting objectively mapped anomalies were added to the 3-month mean density field from SSH alone (i.e., the rightmost term in equation (1)), giving a density field estimate for each 3-month period. The Argo data are too sparse to resolve mesoscale eddies; *Willis et al.* [2003] showed that in the absence of an eddy-resolving observation network, the signal-to-noise ratio of mapped data is significantly improved by removing short-term variability. This is achieved in equation (1) by removing the short-term variability represented by the 7-day SSH-derived estimate of density (i.e., the operation in the curly brackets of equation (1)), and replacing it after mapping the anomalies with the 3-month mean SSH (i.e., the

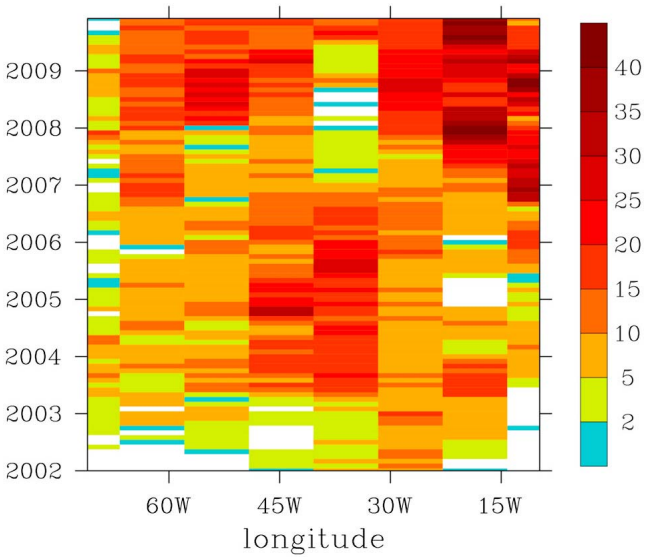

Figure 1. Number of Argo profiles used for each month of the study period in preparation of the gridded density and reference velocity within 380 km of the study section (41°N). Profile counts are grouped into 750 km "bins," i.e., half the zonal covariance length scale estimated by *Willis and Fu* [2008].

rightmost term of equation (1)). By this method, the mesoscale variability in the data was reduced (although not removed entirely) to give a higher signal-to-noise ratio. The effect of removing this short-term variability is discussed at length by *Willis and Fu* [2008] and *Willis et al.* [2003].

[7] Figure 1 shows the number of Argo profiles by month/longitude within a 380 km meridional range of the 41°N section (where 380 km is half of the large-scale meridional covariance scale used in the objective mapping scheme). Most regions have at least 1 observation for each month, but there are data gaps largely close to the boundaries for the first half of the study period, and in the middle of the basin for the latter half of 2007. (Since there is little mid-basin coverage after mid-2006, the failure of a single float could be responsible for the 2007 data gap.) Coverage clearly improved over time, especially in the eastern part of the basin. In regions where there are no Argo profiles at a given time, the mapped state estimates relax to the regression-based SSH-only estimates as described above, thus the SSH data is used to fill gaps in spatial coverage. A similar scheme based on the empirical relationship between SSH and Argo float displacements was used to estimate the 1000 dbar absolute velocity field, which is used for each three-month average as the reference velocity. Figure 2 shows the time-mean 500 m geostrophic velocity of the from the Argo/SSH data in the region of interest. At 41°N (shown by a black line) the Gulf Stream moves away from the western boundary and is in the region observable by Argo floats. Importantly, the longitudes at 41°N with the strongest velocities in Figure 2 (i.e., 30–60°W) correspond to regions with reasonable Argo coverage throughout the study period (Figure 1); where Argo coverage is relatively poor, especially at the western boundary, velocities are quite weak. This suggests that at this latitude the Argo network samples the most important currents in the upper 2000 m.

[8] The estimate of the net MHT is made from the sum of the Ekman, Argo/SSH-observed geostrophic transport, sub-2000 m transport and eddy heat flux components, as summarized by the equation

$$MHT(t) = \int (\rho c_p \theta)_{ek} V_{ek}(t,x)dx + \int_{2000}^{0} \int (\rho c_p \theta V)_{obs} dxdz + \kappa V_{deep} + Q_{eddy} \quad (2)$$

where V_{ek}, V_{obs} and V_{deep} are the Ekman transport, Argo/SSH-observed geostrophic transport and deep ocean transport respectively, κ is the deep ocean volumetric heat content (i.e., $\kappa = \rho c_p \theta$), and Q_{eddy} is the eddy heat flux. Since the individual components of the MHT in equation (2) include nonzero mass transports and are not physically meaningful, here we use the term temperature transport to differentiate the components from the physically meaningful closed-mass heat transport. The first term on the right hand side of equation (2), i.e., the meridional Ekman temperature transport, was calculated using the ECMWF ERA-interim monthly mean zonal wind stress [*Dee et al.*, 2011]. Ekman layer potential temperature, density and specific heat

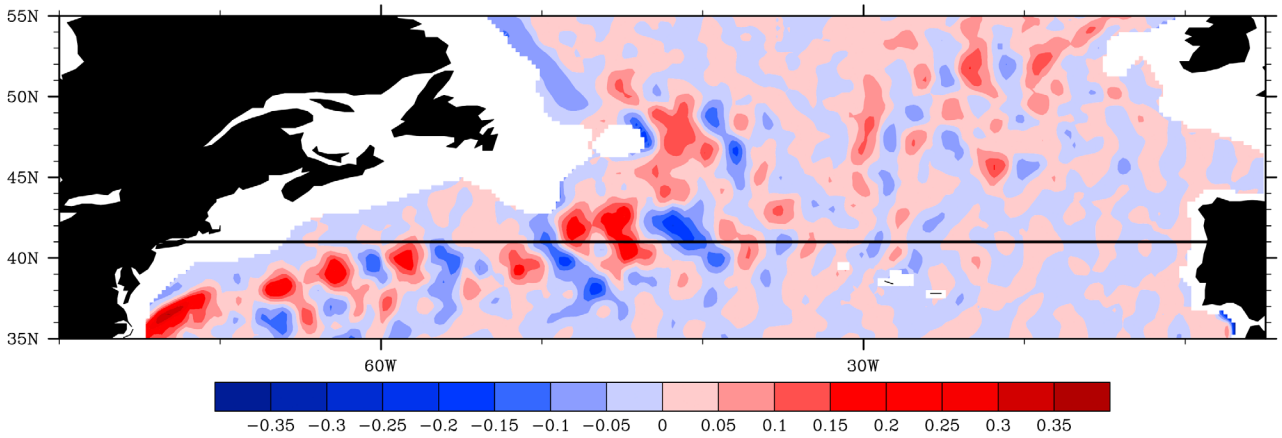

Figure 2. The 2002–2009 mean geostrophic meridional velocity (m s^{-1}) at 500 m depth from Argo/sea surface height (SSH) data.

capacity were estimated as the 0–50 m of Argo/SSH data. The second term in equation (2), the geostrophic temperature transport from the surface to 2000 m, was calculated from the Argo/SSH observations. Using the gridded density estimates to calculate the geostrophic relative velocity and using the 1000 dbar meridional velocity as a reference velocity, the geostrophic northward transport was calculated as described by *Willis* [2010]. This is combined with objectively mapped Argo temperature data to compute the time-varying northward geostrophic temperature transport to a depth of 2000 m.

[9] To calculate the net heat transport, an estimate must be made of the temperature transport below the 2000 m maximum depth of Argo observations (i.e., V_{deep}). This estimate was based on the assumption that there is no net volume transport at each 3-month time step. Thus, the sub-2000 m volume transport was calculated from the total Ekman and super-2000 m observed geostrophic transport, i.e.

$$\int V_{ek}(t,x)dx + \int_{2000}^{0} \int V_{obs}(t,x,z)dxdz + V_{deep}(t) = 0 \qquad (3)$$

where t, x, z are the time, longitude and depth coordinates respectively. Hence, at each time step the total sub-2000 m transport can be estimated. The sub-2000 m water was treated as an isothermal water mass, with a single volumetric heat content, κ (Jm^{-3}). This deep ocean heat content was estimated from the 2009 edition World Ocean Atlas (WOA09 [*Locarnini et al.*, 2010; *Antonov et al.*, 2010]) as the mean of the sub-2000 m heat content, weighted by the magnitude of the meridional mass transport computed from the climatology as discussed in section 3. Transport-weighting was found to be important in estimating the heat content, since the sub-2000 m southward transport generally decreases with depth (Figure 4); unless weighting is used, the average heat content is overly influenced by the cold, deep waters and the heat content is too low. If uncorrected, this reduces the estimated deep southward temperature transport, resulting in a positive bias in the net heat transport estimate. The representative water mass from this flow-weighted mean has a potential temperature of 3.0°C, consistent with North Atlantic Deep Water. Estimates were made for January 2002-September 2010, the period for which Argo data were available.

[10] As described above, eddy variability on time scales of less than 3 months was largely removed from the Argo/SSH data; hence the final term in equation (2), Q_{eddy}, is not directly included in our data. *Volkov et al.* [2008] showed that although eddy fluxes on sub-3 month time scales are important in some latitudes, Atlantic eddy heat flux near 40°N is small.

[11] We estimated this term from the ECCO2 data by calculating the heat flux due to departures from the 3-month mean of the temperature and transport. The ECCO2 data comprise a synthesis of satellite and in situ observations from 1992 to the present, using the MITgcm with an 18 km horizontal resolution in a cube sphere configuration that includes the Arctic Ocean [*Menemenlis et al.*, 2005b]. The subtraction of the 3-month running mean rather than the more conventional long-term mean reflects the fact that eddy fluxes on time scales longer than 3 months are resolved in the Argo/SSH fields. This gave an estimated transient eddy heat flux in the long term mean of 0.05 ± 0.04 PW, which was added to our estimated MHT.

[12] Since Argo floats cannot operate where the total bathymetric depth is less than 2000 m, transport on continental shelves are not included in this estimate. To minimize this source of error, a latitude was chosen with minimal shelf transport. Previous experiments using the ECCO2 global ocean general circulation model have indicated that for the Atlantic, errors due to unobserved shelf transport are minimal in the 40–41.5°N zone [*Willis*, 2010]. This is tested for the heat transport estimate as discussed further in section 3.

3. Validation and Error Estimate

[13] The major sources of uncertainty from the method described above are the sparse Argo float distribution (Figure 1) and unresolved transport on the shallow continental shelf, with further, lesser uncertainties due to the deep ocean flow-weighted heat content and the assumption of zero-net transport integrated over the section. In reality, there is a net transport through the Bering Straits from the Pacific Ocean into the Atlantic basin of approximately 0.7–1.0 Sv [*Woodgate et al.*, 2006]; for the WOA09 climatological temperature, density and heat capacity of the 41°N section, this corresponds to a southward temperature transport of 0.010–0.015 PW. This is not included in the calculation of the MHT described in section 2, but is added to the MHT at each time step. Although there are numerous sources of error in scatterometer-derived wind stresses, a definitive figure for the uncertainty remains elusive. Figure 3 shows the 41°N Ekman transport derived from ERA-Interim monthly mean zonal wind stresses, from the IFREMER Mean Wind zonal wind stress product derived from the NASA QuikSCAT scatterometer (http://cersat.ifremer.fr/) and NCEP-DOE reanalysis [*Kanamitsu et al.*, 2002]. Qualitative comparison of the three products shows that there is little difference in the month-to-month variability, and little bias. The maximum root mean square (RMS) difference between the zonal wind stress products was equivalent to a basin-integrated Ekman transport of 1.46 Sv. As shown in equation (3), an error in the Ekman transport at any time step will be balanced by an error in the sub-2000 m transport of the opposite sign, hence the effect on the MHT is due only to the difference between the temperature of the deep ocean and that of the Ekman layer. As such, an Ekman transport of 1.46 Sv is equivalent to a difference in the net MHT of just 0.09 PW, which we take as our wind stress uncertainty.

[14] Figure 4 shows the profile of the 2002–2009 mean geostrophic temperature transport from the Argo/SSH data, compared with estimates using the World Ocean Circulation Experiment gridded hydrographic climatology (WGHC [*Gouretski and Koltermann*, 2004]) and the WOA09 climatologies. (Argo/SSH data from 2010 was not included to avoid seasonal aliasing due to the unavailability of observations for October–December 2010.) Meridional relative velocities were calculated from the climatological density fields, and the 2002–2009 mean 1000 dbar Argo meridional velocity field was used as a first guess reference velocity. A uniform correction velocity was then added at each grid point to ensure volume transport closure; this correction was

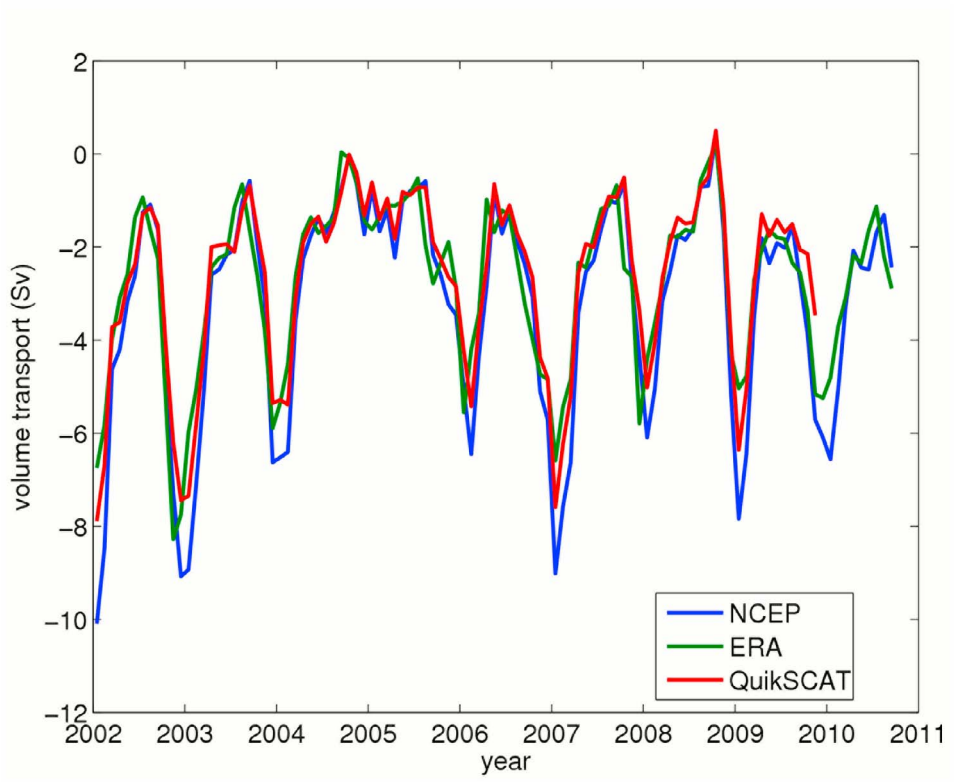

Figure 3. Ekman transport (Sv) at 41°N estimated using QuikSCAT (red line), ERA-Interim (green line), and NCEP2 (blue line).

equivalent to a net transport of −9.5 Sv for the WGHC data, and +12.8 Sv for the WOA09 data. Since the climatologies inevitably share some source observations it may be argued that they are not strictly independent of each other; however, the differences due to processing should give some indication of the robustness of our estimate.

[15] The net heat transports (including Ekman) estimated from the climatologies bound the time-mean Argo/SSH estimate, with a range of 0.33 PW (WGHC) to 0.70 PW (WOA09), compared to the Argo/SSH estimate of 0.48 PW (where eddy heat flux has been excluded since it cannot be resolved by the climatologies). The WGHC heat transport is low compared both to previous calculations (Table 1) and to this study. The upper 2000 m temperature transport profile agrees reasonably well with both climatologies, but the WGHC profile is less than that of the Argo/SSH estimate, and the WOA09 estimate is somewhat greater. Profiles of the volume transport (Figure 4c) show the same basic pattern of biases as the heat transport profiles, indicating that differences in velocity rather than temperature are responsible for the differences in MHT between the two climatologies. To confirm this, net heat transports for the climatologies were also calculated by ignoring the deep climatological density estimate and using the "zero-net volume transport" assumption to estimate transport below 2000 m (i.e., using the Argo/SSH method). Importantly, for both climatologies the result agrees well with the estimate using full depth data (0.30 PW for the WGHC, and 0.63 PW for the WOA09 data), with both Argo/SSH estimates showing a negative bias of ∼10% compared to their respective full-depth climatologies. This suggests that the treatment of the sub-2000 m transport in the Argo/SSH estimate is robust. The surprisingly large difference between MHT of the two climatologies is due mainly to a 4.4 Sv difference in geostrophic transport above 1000 m between the climatologies, and a difference of 3.8 Sv in the Antarctic Bottom Water layer below 4000 m.

[16] The ability of our estimate to represent the temporal variability of the net heat transport was tested using the ECCO2 ocean synthesis. The ECCO2 velocity fields include the ∼1 Sv net southward transport due to Bering Strait throughflow. Since the net heat transport is only meaningful where there is no net mass transport, the residual southward transport at each time step was removed by applying a uniform adjustment velocity to each grid point to achieve balance. The black line in Figure 5 shows the net heat transport calculated using all grid points in the ECCO2 section. The mean heat transport (0.74 PW; dashed black line) is higher than the 2002–2009 Argo/SSH mean, the WGHC or the WOA09 estimates, but is less than the 40°N estimate of *Zheng and Giese* [2009] (Table 1).

[17] To test the assumptions made in estimating MHT using the Argo/SSH data, an "Argo-style" estimate was made from the ECCO2, i.e., by excluding regions where the bathymetry is shallower than 2000 m and all data below 2000 m. As for the Argo/SSH estimate, the net volume closure assumption was combined with a flow-weighted heat content to estimate the ECCO2 heat transport. (Figure 5a, red

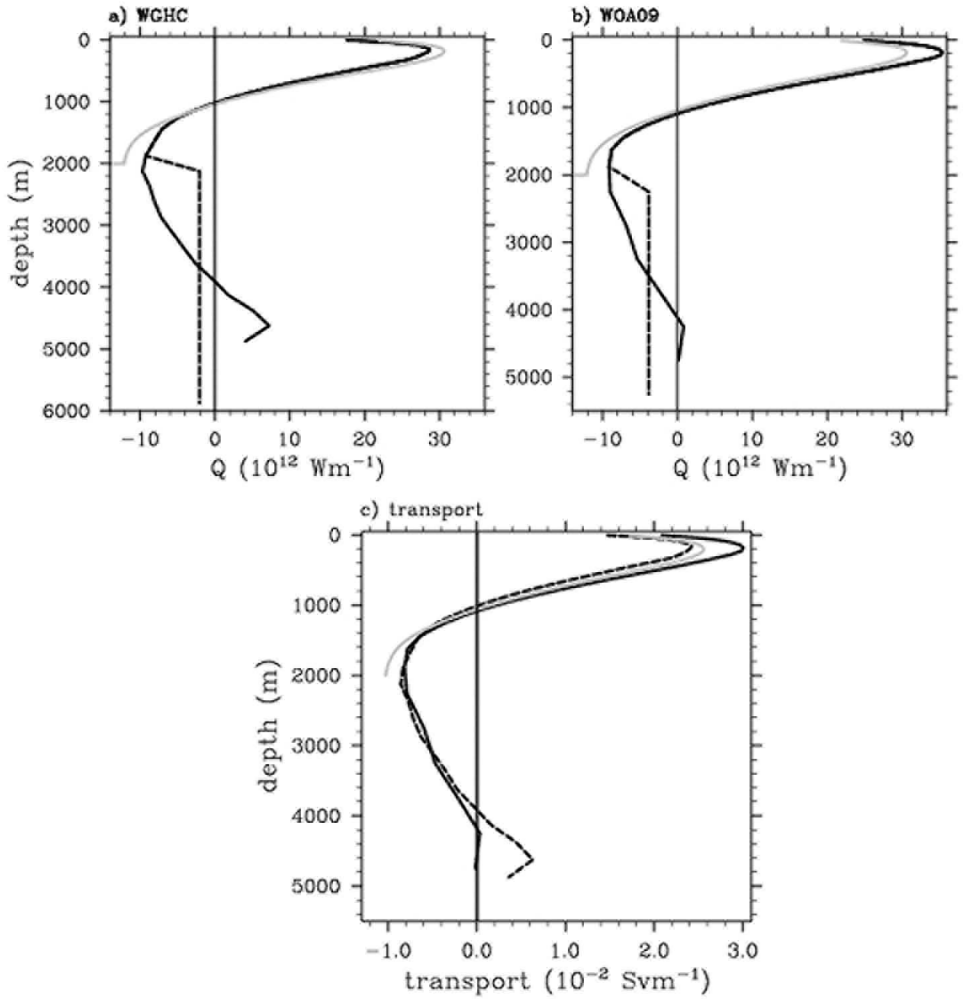

Figure 4. The 41°N basin-integrated geostrophic temperature transport depth profiles (10^{12} W m^{-1}), estimated from (a) WGHC and (b) WOA09 climatologies. Black lines show the heat transport estimated from climatologies throughout the entire depth, gray lines show the 2002–2009 mean Argo/SSH estimate, and dashed black lines show the sub-2000 m transport estimated for the climatologies using the "zero-net transport" assumption. (c) Volume transport per unit depth for WOA09 (solid black line) and WGHC (dashed black line) climatologies, and from Argo/SSH data (gray line).

line). The Argo-style estimate tracks the full-basin heat transport well, with only a 0.08 PW RMS error, and with little bias. The difference between the full-section and Argo/SSH-style estimates is shown in Figure 5b (black line), where it is decomposed into contributions from the shelf regions as well as the deep transport and temperature. Most of the error in the Argo-style estimate is due to the unobserved shelf transport (red line), of which the greatest component is the western boundary (purple line). There is a clear seasonality in the unobserved shelf transport such that the errors are greatest in summer and winter, when western shelf temperature transport is at its seasonal minimum/maximum respectively.

[18] The western shelf at this latitude includes the Georges Bank, for which several experiments have measured along-shelf transport, but also includes a largely unobserved region between the Georges Bank and Long Island [*Lentz*, 2008]. However, current meter data are available for approximately 39°N from repeat tracks of the line W section (*Peña-Molino and Joyce* [2008]; http://www.whoi.edu/science/PO/linew/). Since in the ECCO2 model the total unobserved western boundary transport at 41°N is similar that across the line W track (-1.28 ± 3 Sv at 41°N, compared to -1.18 ± 4 Sv across line W), we argue that an estimate from line W observations is sufficient to test whether the ECCO2 error is reasonable. Figure 6 summarizes the estimate of shelf and slope transport for Line W. We estimated unobserved slope transport (i.e., transport integrated from the shelf break to the 2000 m isobath) using 14 repeat sections from December 1995 to May 2008 (Figure 6, red line); transport along the shelf was estimated using the empirical relationship between depth and across-shelf transport of *Lentz* [2008] (blue line, Figure 6). This method gave an estimate of 0.45 ± 3 Sv for the slope transport, and -0.82 Sv for the shelf transport, giving a total of -0.37 Sv not observed by Argo. (Note that the Lentz relationship is time-invariant, and gives no information about variability). This value is well within the range

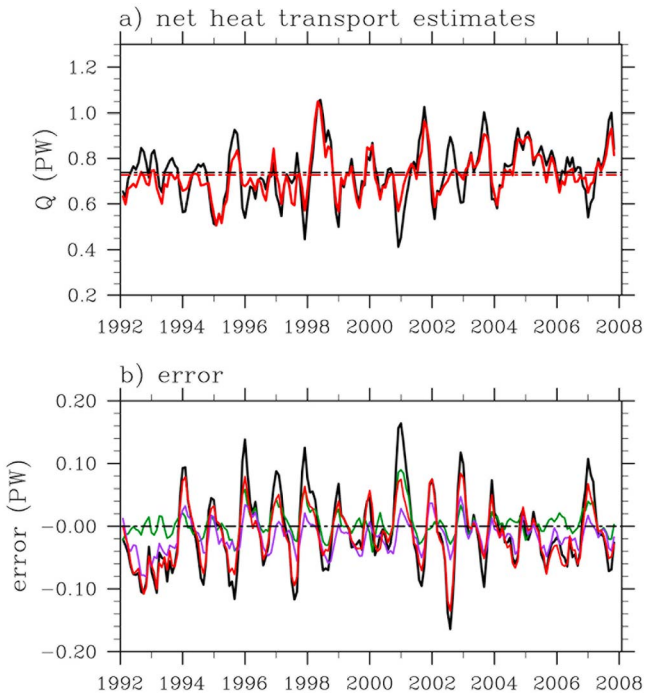

Figure 5. The 41°N net meridional heat transport estimated from the ECCO2 model. (a) Net heat transport estimated using all data points along section (black line), and using data points covered by Argo floats, where zero-net volume transport is used to estimate sub-2000 m heat transport (red line); dashed horizontal lines show the mean for each estimate. (b) Difference between full-section heat transport estimate and Argo/SSH-style estimate (black line). This error is further decomposed into contributions from the sub-2000 m flow-weighted heat content (green line), unobserved shelf transport (red line), and unobserved American shelf transport (purple line).

of the ECCO2 estimate, suggesting the simulated error due to unobserved western boundary transport is reasonable. For a mean shelf water temperature of 11°C (estimated from the NOAA Optimal Interpolation sea surface temperature v2 [*Reynolds et al.*, 2002]), and a mean slope water temperature of 6°C (estimated from Line W temperature data), this results in a MHT bias of approximately -0.018 ± 0.04 PW; for comparison, the ECCO2 experiment gave a bias due to western shelf transport of -0.016 ± 0.03 PW.

[19] The uncertainties due to using a constant sub-2000 m flow-weighted volumetric heat content come from unresolved time variations in the heat content, and from the estimate of the constant heat content itself. The green line in Figure 5b shows the error in the ECCO2 experiment due to heat content variability, which is only significant when the net heat transport is large. When the strength of the overturning is relatively large (and therefore so is the deep southward return flow), differences between the actual and observed deep ocean heat content are multiplied by a larger transport; hence, the uncertainty due to the flow-weighted volumetric heat content is magnified when the AMOC is strong. This underscores the need to make periodic measurements of the deep ocean temperature and salinity structure over time. In the ECCO2 model the RMS error due to the deep ocean heat content is 0.03 PW, with no bias. There is also an uncertainty in the estimate of transport-weighted heat content from climatological data. The difference between the transport-weighted heat contents calculated from the WOA09 and WGHC climatologies was equivalent to a temperature difference of less than 1°C, which for a time-mean sub-2000 m southward transport of 5.1 Sv (as calculated from equation (3) using Argo/SSH and era wind stress data), would result in an error in net MHT of 0.02 PW. Combining these numbers gives an uncertainty due to the unobserved deep ocean of 0.036 PW.

[20] The largest source of uncertainty in the heat transport is due to sampling error. This is calculated based on the skill computed as part of the objective mapping of Argo temperature, density and the 1000 dbar reference velocity, and estimating the influence of these terms on the heat transport estimate. The skill is defined as one minus the ratio of the estimated variance to the error variance. *Willis and Fu*

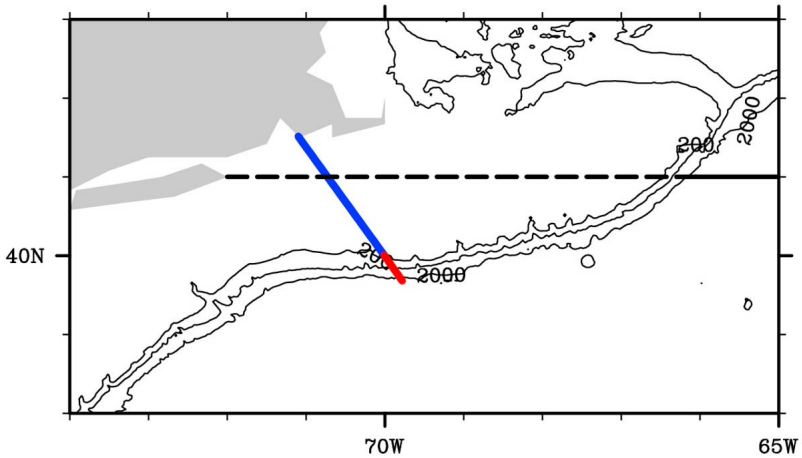

Figure 6. Bathymetric map summarizing line W estimate of unobserved shelf transport. Black line shows 41°N section and is dashed where bathymetry is less than 2000 m; red line shows continental slope from shelf break to 2000 m isobath as observed by line W current meters; blue line shows extension of line W along continental shelf where transport was estimated using *Lentz* [2008]. Contours show the 2000 m, 1000 m, and 200 m isobaths.

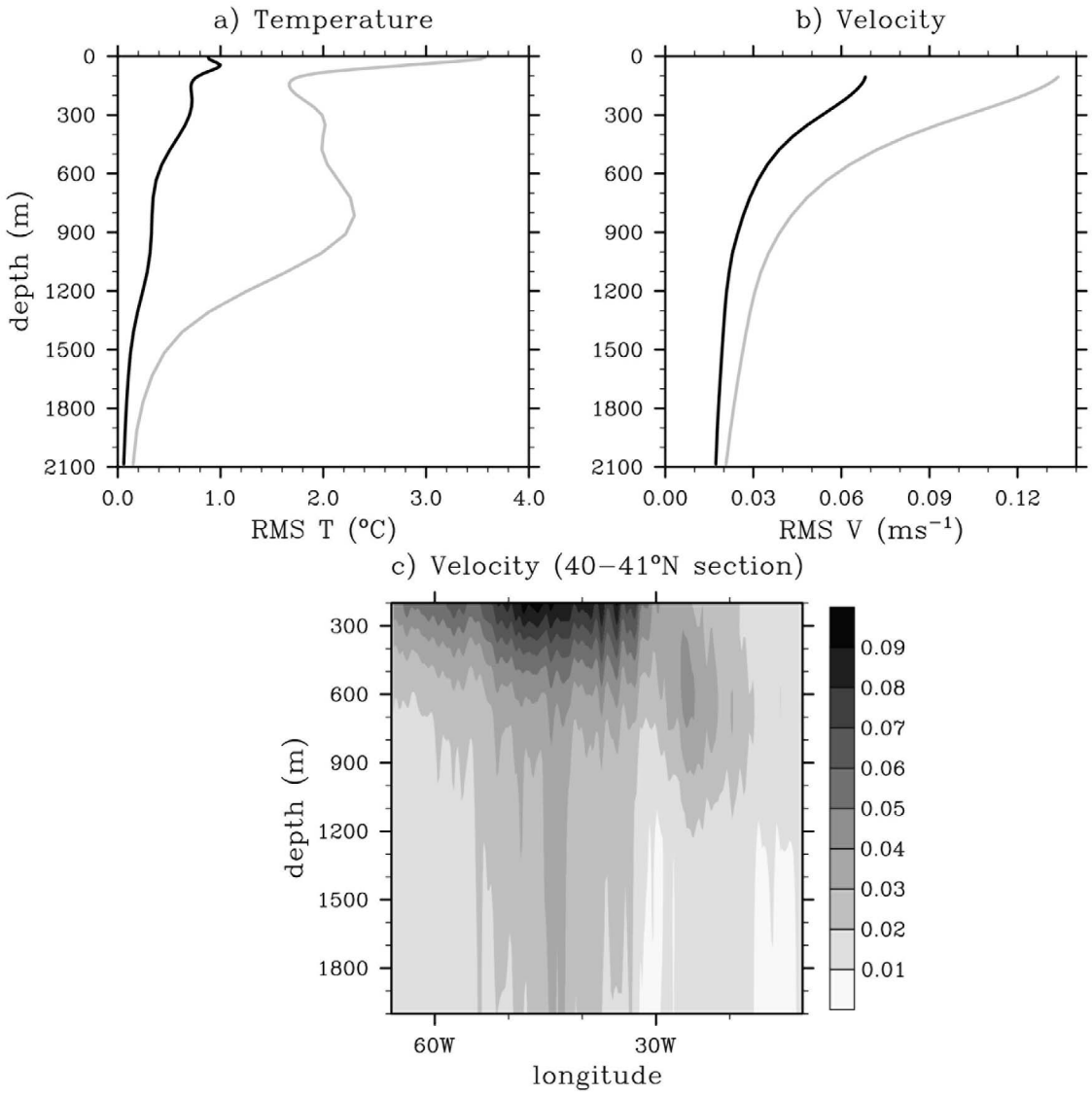

Figure 7. Vertical profiles of (a) temperature (°C) and (b) velocity (m s^{-1}) root mean square differences between sampled and unsampled ECCO2 fields (black lines), for the domain 40–45°N. Gray lines show standard deviations of the unsampled data. (c) Root mean root mean square difference in velocity for the 40–41°N latitude domain.

[2008] found that for their choice of mapping parameters in this region, the skill could be used as an accurate measure of sampling error. The heat transport error due to data sampling is approximately 0.18 PW for most of the 3-month average time steps, which is significantly greater than the errors due to wind stress uncertainty or the heat transport estimation method. This uncertainty ranges from 0.15 to 0.19 PW, depending on data coverage (Figure 1).

[21] The sampling error was also estimated using 3-day averaged fields from the ECCO2 simulation. Using actual Argo profile times and locations as starting points, 9-day 1000 dbar trajectories were computed from the model velocity fields using a fourth-order Runge–Kutta method to give a final profile location. Argo trajectories have an uncertainty due to the unknown drift during ascent/descent, and drift while on the surface. To simulate this, random normal error with a mean of 0 and a standard deviation of 1900 m was added to each trajectory's zonal and meridional displacements (where a 1900 m displacement in each direction corresponds to a total uncertainty of 2.7 km, as calculated by *Willis and Fu* [2008]). Thus for each real Argo location, a simulated trajectory and corresponding T/S profile was computed. Combining these data with the simulated SSH in exactly the same way as is done for the real Argo floats, estimates of temperature, salinity, density and 1000 dbar reference velocity were computed which were compared with the ECCO2 "truth." Figures 7a and 7b show the vertical distribution of RMS differences between the samples and unsampled cases for geostrophic velocity and potential temperature, for the Atlantic Ocean at 40–45°N. For both quantities the RMS error is less than the standard deviation, implying some skill in estimate the temperature

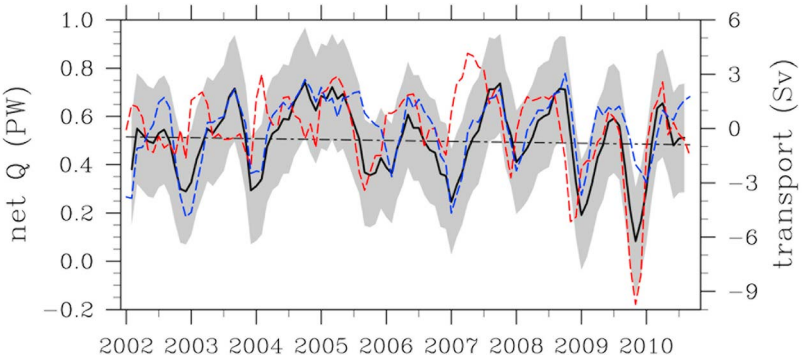

Figure 8. Net heat transport at 41°N estimated from Argo and SSH observations (black line, left *y* axis), with systematic uncertainty shown by gray shading. The dashed black line shows the estimated linear trend. Dashed curves (right *y* axis) show upper 1130 m geostrophic (red) and Ekman (blue) transports (Sv), having removed the long-term mean (17.5 Sv for the geostrophic and −2.8 Sv for the Ekman transports).

and velocity fields. The spatial distribution of velocity RMS error along the 40–41°N transect is shown in Figure 7c, and it can be seen that the greatest errors are concentrated in the 30–60°W longitude zone, where the Gulf Stream passes through the transect (Figure 2), and variability is therefore greatest. This also corresponds to the latitude of relatively high Argo float density (Figure 1), implying that the relative sparse Argo observations near the western boundary are not the major source of sampling error.

[22] Using time-mean density, specific heat capacity, and as appropriate transport or temperature data from the actual Argo/SSH data, a heat transport was calculated for a transport or temperature profile equal to the uncertainties shown in Figure 7, to give subsequent MHT of 0.03 PW due to uncertainty in temperature sampling, and 0.19 PW due to geostrophic velocity (noting that the velocity uncertainty includes errors from both the density field and the 1000 dbar velocity), giving a total sampling error of 0.22 PW. These errors are random, and no bias was found due to the sampling scheme. Therefore, we argue that these values are consistent with the 0.18 PW sampling error estimated from the objective mapping scheme skill scores.

[23] Combining the 0.18 PW sampling error with uncertainty in eddy heat flux (0.04 PW), Ekman transport (0.09 PW) and the MHT calculation assumptions (0.09 PW), and assuming that these error sources are uncorrelated, gives a systematic uncertainty of 0.22 PW for each time step's estimate. The autocorrelation functions of the sampling and calculation assumption errors indicate that 6 months is a conservative decorrelation time for the errors, where the 3-month averaging period has been accounted for; this gives 14 degrees of freedom over the 7 complete years of available data, and thus a systematic uncertainty in the mean MHT of 0.06 PW. The net sum of biases due to unobserved shelf transport, Bering Straits throughflow and unresolved eddy fluxes was 0.02 PW, which was added to the heat transport estimates.

4. Results

[24] The 2002–2009 mean net heat transport for 41°N is estimated from Argo/SSH data as 0.50 PW, including eddy heat flux (where again 2010 is omitted from this mean estimate to avoid seasonal biases). The heat transport shows a high degree of variability, with a total range over the study period of −0.88–1.01 PW, and a standard deviation of 0.18 PW. The decorrelation time for the MHT time series is 5 months, which combined with the standard deviation gives a statistical uncertainty (i.e., uncertainty due to natural variability in the MHT) of 0.05 PW for the time-mean estimate of MHT. Combining this with the systematic error gives a total uncertainty in the MHT of 0.1 PW for the mean over 7 years. (It should be noted that since decadal variability cannot be included in our estimate of the standard deviation, the true statistical uncertainty of a long-term mean could well be higher).

[25] There is a slight, statistically insignificant negative trend in heat transport over the study period equivalent to -0.05 PW decade^{-1}. The heat transport time series is shown in Figure 8, with the Ekman and upper 1130 m geostrophic volume transports; since 1130 m is the approximate level of zero northward transport for the overturning circulation at this latitude [*Willis*, 2010], the Ekman and geostrophic transports above this level give a good indication of the variability in northward AMOC strength. Cross-correlations of the MHT with the Ekman and upper 1130 m geostrophic volume transports indicate that 51% of the MHT variability is explained by Ekman transport, as opposed to just 19% for the upper 1130 m geostrophic transport. (Note that this is for timescales of 3-months or longer as resolved by the Argo/SSH data; on shorter timescales Ekman transport would be expected to explain a higher fraction of MHT variance.) Interestingly, on interannual timescales there is a statistically significant correlation (r = 0.25) between the Ekman and geostrophic transports so that a decomposition into MHT variances-explained is difficult; however, we note that there is a higher correlation with annual-mean MHT for the geostrophic transport (r = 0.77) than for the Ekman transport (r = 0.66). The correlation between the Ekman and geostrophic components suggests that wind-driven changes in hydrography may act to adjust the geostrophic transport.

[26] The annual cycles of the MHT and Ekman and geostrophic transports are shown in Figure 9, where the seasonal cycle was calculated as the average over the 8-year analysis

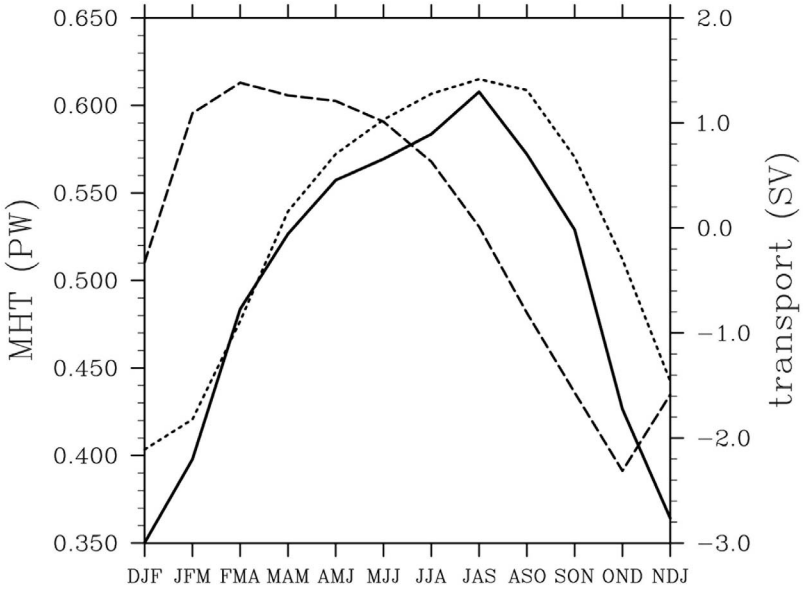

Figure 9. The 2002–2009 annual cycles of net heat transport (black line, left *y* axis), and the Ekman (dotted) and upper 1130 m geostrophic (dashed) transport (right *y* axis, Sv). (For comparison, the long-term means have been removed from the volume transports.)

period of each 3 month seasonal mean. The Ekman and geostrophic transports have similar amplitudes of seasonality, but the cycle of MHT closely corresponds to that of the Ekman transport. This is confirmed by correlation of the seasonal cycles, which indicates that 81% of the MHT seasonality is explained by the Ekman component. The Ekman transport is most positive during the summer (Figure 9, dotted line); since summer zonal winds are relatively weak, the southward (i.e., negative) Ekman transport is low. The geostrophic transport's seasonal cycle (dashed line) leads that of the Ekman component, with a peak in March, and trough in November. An interesting comparison can be made with the seasonal cycle at 26.5°N. *Johns et al.* [2011] found a seasonal cycle with a minimum in March, when the MHT at 41°N is relatively high. Additionally the amplitude of the seasonal cycle at 26.5°N is approximately double that of 41°N, being in excess of 0.5 PW [*Johns et al.*, 2011]. At 26.5°N the MHT seasonal cycle has significant contributions from both the Ekman and geostrophic components which are roughly in phase with each other, possibly explaining the stronger seasonal cycle at that latitude, compared to 41°N where these components are out of phase. At 41°N the Ekman temperature transport has much greater seasonal amplitude than at 26.5°N, reflecting the greater zonal wind seasonality in the mid latitudes. It is also interesting that the geostrophic component at 26.5°N is at its minimum in March [*Kanzow et al.*, 2010; *Johns et al.*, 2011], when the 41°N geostrophic transport is close to its maximum. We note that at both latitudes the seasonal cycles are related to the annual evolution of the winds, whether through Ekman transport or Ekman pumping.

5. Discussion

[27] Table 1 shows previous estimates of midlatitude North Atlantic MHT by latitude. In the rightmost column, we adjust our mean value of 0.50 PW to latitude by adding the mean surface flux between 41°N and the appropriate latitude, and assuming no long-term change in ocean heat storage. Annual-mean surface heat fluxes were taken from the National Oceanography Centre flux (NOCflux) climatology [*Grist and Josey*, 2003] (see Figure 10). Our estimate is consistent with the geographically closest previous heat transport estimates derived from surface fluxes [*Hsiung*, 1985; *Trenberth and Caron*, 2001], but is much less than 1.09 PW estimate from ocean reanalysis data [*Zheng and Giese*, 2009]. The Zheng and Giese analysis shows an increase in MHT between 30 and 40°N, which implies an input of heat from ocean to atmosphere between these latitudes; this is not borne out by surface flux estimates, and challenges the reliability of MHT in ocean reanalysis data. Compared to hydrographic estimates, however, our value is low. The 36°N section has been studied for some time, with estimates close to either 0.8 PW [*Roemmich and Wunsch*,

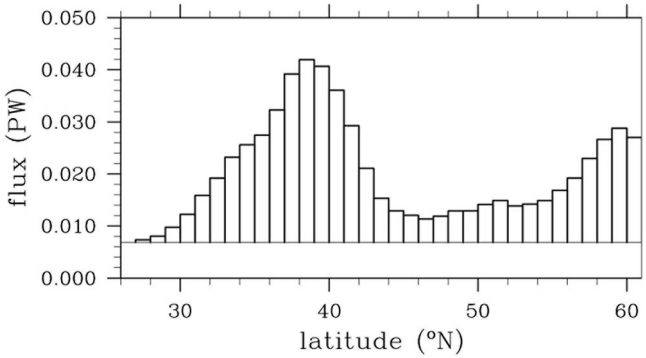

Figure 10. North Atlantic ocean-to-atmosphere net surface heat flux (PW) integrated over 1 degree latitude, from the NOC flux climatology [*Grist and Josey*, 2003].

1985; *Talley*, 2003] or 1.2 PW [*Rintoul and Wunsch*, 1991; *Sato and Rossby*, 2000; *McDonagh et al.*, 2010]. Within the range of uncertainty our estimate is consistent with an MHT at 36°N of ~0.8 PW, but not 1.2 PW. We find North of 41°N our estimate again seems generally low compared to those based on hydrographic data, with the exception of that of *Bacon* [1997].

[28] An important question is whether this under-estimate is due to systematic bias in the Argo/SSH calculation method. It should be noted that our calculation method is fundamentally different from those using hydrographic data since known reference velocity computed from Argo float displacements were used; for hydrographic calculations where the reference velocity is not known an inverse box model based on conserved tracers must be employed. Furthermore, hydrographic estimates are based on a single observation period, whereas our estimate includes variability in inter-seasonal to inter-annual time scales. *Koltermann et al.* [1999] made estimates using repeat hydrographic sections that were in the range 0.47–1.29 PW at 36°N, over the 1957–1993 time period. While some of this range is no doubt due to decadal variability that the Argo data cannot yet resolve, it clearly highlights the sensitivity of hydrographic calculations to synoptic variability. Both this research and work by *Kanzow et al.* [2010] show that there is a strong seasonal cycle in Atlantic MHT. Most hydrographic surveys are carried out during the temperate summer months, when our results indicate that MHT is climatologically greatest (the May–July MHT at 41°N is 0.57 PW), which could imply a seasonal bias in the hydrographic estimates. However, most estimates use a time-mean Ekman transport in the solution of an inverse box model, and as previously shown the annual cycle at 41°N is largely due to Ekman transport variability. For fair comparison, we recalculated the MHT using a time-mean Ekman temperature and volume transport, and found that the May–July mean without the Ekman annual cycle is a little higher than the long-term mean (0.52 PW), but this difference does not explain the discrepancy with hydrological estimates.

[29] Both *Rintoul and Wunsch* [1991] and *McDonagh et al.* [2010] suggested that the roughly 0.4 PW difference in estimates for the relatively well-observed section at 36°N could be from an underestimate of the horizontal heat transport component, which they attributed to smoothing in the treatment of hydrographic data in the lower estimates. We calculated the horizontal and overturning components in the Argo/SSH estimate using the same decomposition as *McDonagh et al.* [2010], where the horizontal heat transport is calculated from the zonal anomalies of the temperature and velocity fields, and the overturning transport is calculated from the temperature and velocity zonal means. (Of course the Argo data can only observe horizontal transport to 2000 m, but the horizontal component below this depth should be relatively low.) The mean horizontal transport at 41°N was 0.04 PW, an order of magnitude lower than *McDonagh et al.*'s [2010] estimate for 36°N. However, since 41°N is in the "inter-gyre" region between the subpolar and subtropical gyre a weak horizontal heat transport would be expected. Furthermore, we note that for 26°N *Johns et al.* [2011] found a horizontal heat transport of 0.15 PW despite being in a region with a significant gyre, suggesting that there is a high degree of latitudinal variability in the Atlantic horizontal heat transport component. Therefore there is no strong evidence that the low MHT at 41°N is underestimated due to unresolved horizontal heat transports.

[30] Another possible reason for the relatively low estimate is the complexity of the region of interest, which has strong meridional temperature gradients. Figure 10 shows a clear reduction in ocean-to-atmosphere heat flux between 39 and 42°N, implying a large meridional difference in heat transport. Using Argo/SSH data, we calculated the difference in average ocean heat content above 1130 m between 40 and 41°N. Taking a time-mean Ekman transport of −2.8 Sv from the ERA wind stress data, a geostrophic transport 16.2 Sv, and assuming that the meridional temperature gradient in the deep ocean is relatively weak, this temperature gradient gives a reduction in MHT of 0.06 PW from 40 to 41°N; the NOCflux surface flux between these two latitudes is just 0.03 PW. While this calculation is rather simple, it does suggest that there may be meridional heat flux variability that the surface flux estimates cannot resolve. *Lozier et al.* [2010] showed that late 20th century trends in the subpolar and subtropical gyres were not even of the same sign, while model experiments with both fully coupled and ocean-only models have indicated that the 40°N latitude marked a shift in the Atlantic's dynamic regime [*Bingham et al.*, 2007]. Given the complexity of the region and the uncertainties in the surface flux, the relatively low MHT observed in the present study may not be unreasonable.

[31] The only other time-varying estimate of the Atlantic MHT is from data collected by the RAPID-MOCHA array at 26.5°N [*Johns et al.*, 2011]. The heat transport at that latitude is generally higher than at 41°N, and as noted its variability may be in a different physical regime. It is however instructive to compare the variance characteristics for the two estimates. As expected, the mean heat transport at the RAPID array is higher than at 41°N (1.33 ± 0.14 PW), as is the standard deviation (0.4 PW), although it should be noted that the *Johns et al.* [2011] estimate includes variability on 1–3 month timescales that our MHT cannot resolve. Having filtered short-term variability with a 3-month moving average, the standard deviation of the Johns et al. MHT time series is significantly reduced to 0.25 PW, similar to the 0.2 PW standard deviation at 41°N. Previous research on the meridional coherence of the AMOC has largely relied on model simulations, but with continued measurements at different latitudes from the Argo and RAPID observing systems, an observation-based study seems feasible.

[32] One of the major motivations for monitoring the Atlantic MHT is to understand the impact of Atlantic Ocean variability on Northern Hemisphere climate. Much of this impact is believed to occur at multidecadal or longer time scales [e.g., *Knight et al.*, 2005], which clearly cannot be resolved at this time due to the short observation period. However, it is interesting to consider the possible shorter-timescale impacts of the MHT. Assuming negligible energy flux through the Straits of Gibraltar, the difference between our estimate of MHT at 41°N and that of *Johns et al.* [2011] for 26.5°N implies a mean energy convergence of 0.83 ± 0.17 PW between these latitudes, significantly higher than the 0.36 PW suggested by the mean surface net flux between these latitudes. This energy must be partitioned between an increase in local ocean warming in the 26.5–41°N region,

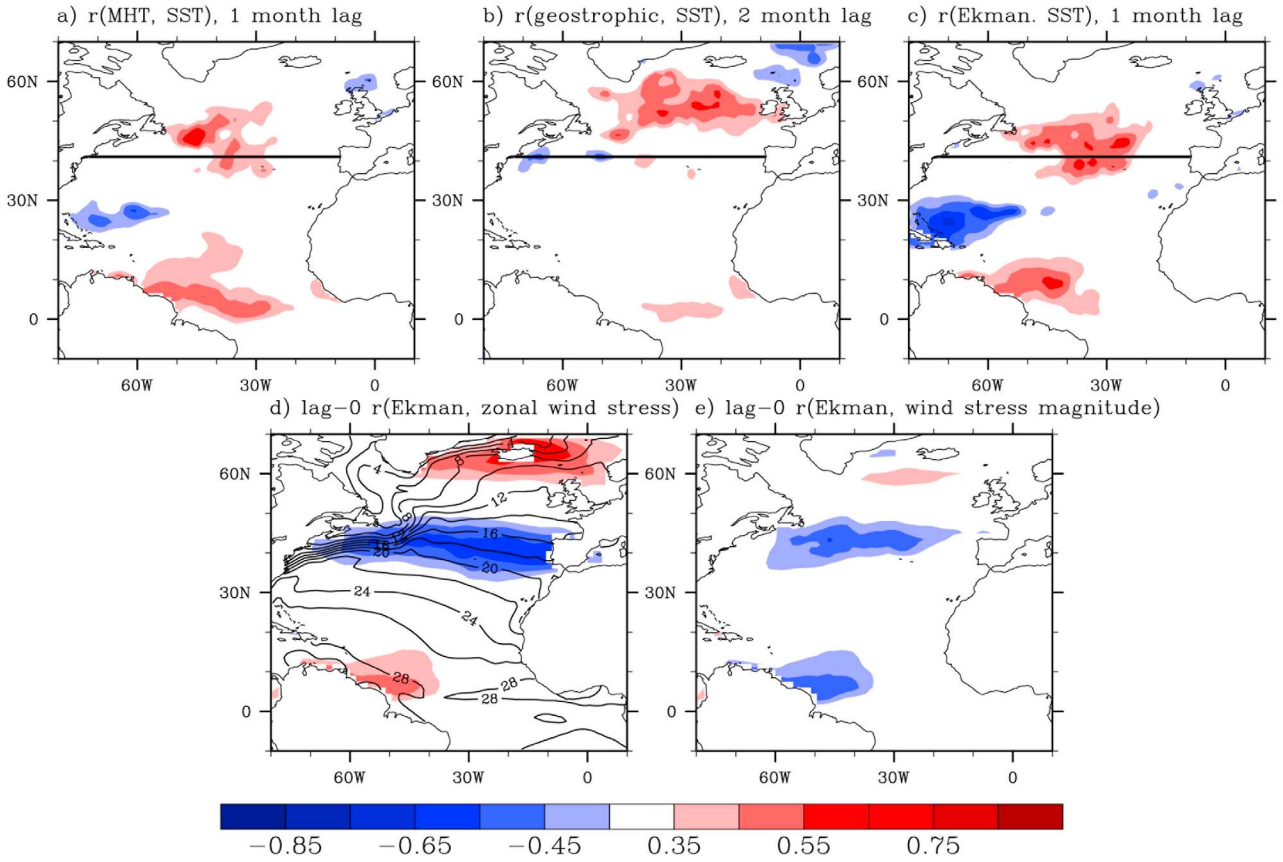

Figure 11. Lagged correlations of OIv2 SST with (a) heat transport at 1 month lag, (b) geostrophic temperature transport at 2 month lag, and (c) Ekman temperature transport at 1 month lag; solid black line shows the 41°N section. (d) Zero-lag correlation between Ekman temperature transport and zonal wind stress, with contour lines showing the time-mean SST (°C). (e) Zero lag correlation between Ekman temperature transport and wind stress magnitude. Trends and annual cycles were removed from all data before correlations, and a 3-month running average was applied to the wind stress and SST data to match the 3-month averaged transport time series. All shaded correlations are significant at the 0.05 level or greater.

and ocean-to-atmosphere energy flux. Since long-term trends in ocean heat are small compared to the long-term mean, it is implied that much of this energy convergence must be released to the atmosphere. If the AMOC variability indeed has an influence on the Northern Hemisphere climate, it must be through changes in the sea surface temperature (SST), which impact the distribution of ocean–atmosphere surface heat fluxes. The heat transport was correlated with the NOAA Optimal Interpolation SST v2 [*Reynolds et al.*, 2002]. Before correlations were computed, the trend and seasonal cycle were removed from both data sets. Due to the relatively short time period, a resampling approach was used to estimate statistical significance using the technique of *Hobbs and Raphael* [2010]. Analysis of the autocorrelation functions of the deseasoned MHT, Ekman and geostrophic temperature transports could be modeled as autoregressive processes of order 5, 1, 3, and 6 respectively. For each time series, 1000 random samples with the same length, standard deviation and autocorrelation functions as the original time series were generated. These were correlated with similarly generated resampled SST time series to give 10^6 correlation coefficients, giving probability density functions of the correlations between SST and the initial time series. The 95-percentile correlation coefficients (i.e., the correlation coefficient at which correlations were significant at the 0.05-level) were taken from these probability density functions. Using this criterion, for the MHT and geostrophic temperature transport time series correlations exceeding 0.35 were significant, and for the Ekman temperature transport correlations exceeding 0.27 were significant.

[33] Correlations were performed for a range of lags up to 60 months, with the strongest correlations occurring for heat transport leading SST by 1 month (Figure 11a). The correlation pattern is marked by a positive relationship between heat transport and SST at 30°W, 40–50°N, with evidence of a teleconnection with SST off the Florida Keys and the northwest South America. The correlation analysis was repeated using the Ekman and geostrophic temperature transports. The geostrophic transport has its greatest impact after 2 months (Figure 11b), and shows a warming in the North Atlantic consistent with the transport of warm water northward from 41°N. However, the pattern does not correspond to that of the total heat transport, which is much better explained by the Ekman component (Figure 11c). The influence of the Ekman component was further explored by making a zero-lag correlation of Ekman temperature transport

with the zonal wind stress and the wind stress magnitude. (Note that for the correlations with wind stress a coefficient of 0.23 was found to be significant at the 0.05-level, somewhat lower than the minimum correlations shown here.) The correlation with zonal wind stress (Figure 11d) shows strong anomalies across width of the Atlantic basin, indicating a North Atlantic Oscillation-like shift in the mid latitude jet stream. At 41°N the Ekman component is high (or more specifically, less negative) when local zonal wind stress is weak, causing a reduced southward flow. Although the wind stress signal is coherent across the basin, the SST response to Ekman variability in Figure 11c is concentrated mid-basin, and this appears to be due to the mean distribution of SST (shown by contour lines in Figures 11d and 11e); the mid-latitude Ekman response is greatest where the meridional SST gradient is strongest, between 30 and 50°W. The wind stress magnitude (Figure 11e) also shows a reduction when the Ekman component is strong, which is concentrated in the region of greatest SST-response (Figure 11c). This reduction in wind stress would lead to a local reduction in ocean cooling by surface heat flux, which in turn is consistent with an increased SST. Because of the relatively short time scales involved, the apparent SST responses in the western tropical Atlantic are most likely explained by the large scale atmospheric variability. Both the magnitude and zonal component of wind stress show zero-lag responses in the region of the teleconnected SST response (Figures 11d and 11e), implying that a single, large-scale mode of atmospheric variability is at play, rather than a coherent AMOC response. In summary, it appears that at the time scales observable by the Argo/SSH data, much of the SST-response to MHT variability is best explained by atmospheric variability, through surface heat and momentum fluxes. These results are preliminary given the short period of available data, and further work will be required as more Argo data become available to confirm physical relationships suggested here. In particular, the geostrophic temperature transport component is likely to have a more important climate impact at longer time scales than are currently observed by the Argo network.

6. Conclusions

[34] We have presented a novel method of deriving the North Atlantic MHT from Argo and satellite data for a specially chosen location in the mid latitude North Atlantic, which employs reference velocities derived from Argo float data rather than the use of an inverse model. This provides one of only two continuous time series of heat transport (the other being from the RAPID array), and is the longest such estimate to date. The assumptions in our calculation have been tested using hydrographic climatologies and model simulations and are shown to be valid. The largest source of error is due to the sparse spatial distribution of Argo float profiles.

[35] Our mean estimate of 0.50 $\pm$ 0.1 PW for the 41°N heat transport is consistent with previous studies in similar latitudes based on atmospheric flux data, but is low compared with hydrographic estimates. It is unclear whether this estimate is relatively low due to bias in the method, deficiencies in surface heat flux data, or is due to the high the temporal and spatial variability of Atlantic MHT. Although the uncertainty in our estimate is not appreciably less than for previous studies based on a few hydrographic sections, the high variability shown by our time series suggests that those earlier calculations may have underestimated statistical uncertainty. In spite of the relatively short time period of available observations, the heat transport time series shows a statistically significant relationship with North Atlantic SST variability. Although preliminary, these correlations indicate some interesting relationships that merit further investigation as more observations become available.

[36] Due to its profound influence on the Northern Hemisphere climate and its potential response to climate change, there is a pressing need for continuous monitoring of the AMOC using schemes such as the estimate presented here, or the lower-latitude RAPID array. In this work we employed a line of opportunity due to its relatively weak shelf transport, although it seems feasible that western boundary observations, for example those at Line W, could be combined with Argo/SSH data to open up further latitudes of opportunity for AMOC/MHT observation. Reliable time-varying estimates of Atlantic heat transport are important for climate change detection, ocean model validation, and climate analysis. At present these continuous observations are too short to capture multidecadal variability, the time scale at which the impact of natural AMOC fluctuations on climate are believed to be strongest. However, it is hoped that the ability to derive physically meaningful time-dependent estimates should be a forceful argument for the continued maintenance of existing observing systems.

[37] **Acknowledgments.** The authors wish to thank W. Johns for helpful discussions over the course of this work, and for supplying MHT data from the RAPID array. We also thank three anonymous reviewers. Altimeter products were produced by Ssalto/Duacs and distributed by Aviso with support from CNES. Argo data were collected and made freely available by the International Argo Project (http://www.argo.ucsd.edu). Scatterometer products were produced and distributed by IFREMER. Data analysis was performed using the NCAR Command Language (http://www.ncl.ucar.edu). This work was carried out at the Jet Propulsion Laboratory, California Institute of Technology, under a contract with NASA.

References

Antonov, J. I., D. Seidov, T. P. Boyer, R. A. Locarnini, A. V. Mishonov, H. E. Garcia, O. K. Baranova, M. M. Zweng, and D. R. Johnson (2010), *World Ocean Atlas 2009*, vol. 2, *Salinity*, edited by S. Levitus, 184 pp., U.S. Gov. Print. Off., Washington, D. C.

Bacon, S. (1997), Circulation and fluxes in the North Atlantic between Greenland and Ireland, *J. Phys. Oceanogr.*, *27*, 1420–1435, doi:10.1175/1520-0485(1997)027<1420:CAFITN>2.0.CO;2.

Bingham, R. J., C. W. Hughes, V. Roussenov, and R. G. Williams (2007), Meridional coherence of the North Atlantic meridional overturning circulation, *Geophys. Res. Lett.*, *34*, L23606, doi:10.1029/2007GL031731.

Cunningham, S. A., et al. (2007), Temporal variability of the Atlantic meridional overturning circulation at 26.5°N, *Science*, *317*, 935–938, doi:10.1126/science.1141304.

Dee, D. P., et al. (2011), The ERA-Interim reanalysis: Configuration and performance of the data assimilation system, *Q. J. R. Meteorol. Soc.*, *137*, 553–597, doi:10.1002/qj.828.

Delworth, T. L., and M. E. Mann (2000), Observed and simulated multidecadal variability in the Northern Hemisphere, *Clim. Dyn.*, *16*, 661–676, doi:10.1007/s003820000075.

Folland, C. K., D. E. Parker, and T. N. Palmer (1986), Sahel rainfall and worldwide sea temperatures, 1901–85, *Nature*, *320*, 602–607, doi:10.1038/320602a0.

Folland, C. K., A. W. Colman, D. P. Rowell, and M. K. Davey (2001), Predictability of northeast Brazil rainfall and real-time forecast skill, 1987–98, *J. Clim.*, *14*, 1937–1958, doi:10.1175/1520-0442(2001)014<1937:PONBRA>2.0.CO;2.

Ganachaud, A., and C. Wunsch (2003), Large-scale ocean heat and freshwater transports during the World Ocean Circulation Experiment, *J. Clim.*, *16*, 696–705, doi:10.1175/1520-0442(2003)016<0696:LSOHAF>2.0.CO;2.

Goldenberg, S. B., C. W. Landsea, A. M. Mestas-Nunez, and W. M. Gray (2001), The recent increase in Atlantic hurricane activity: Causes and implications, *Science*, *293*, 474–479, doi:10.1126/science.1060040.

Gouretski, V. V., and K. P. Koltermann (2004), WOCE global hydrographic climatology, *Tech. Rep. 35*, 52 pp., Bundesamt für Seeschifffahrt und Hydrographie, Hamburg, Germany.

Gregory, J. M., et al. (2005), A model intercomparison of changes in the Atlantic thermohaline circulation in response to increasing atmospheric CO_2 concentration, *Geophys. Res. Lett.*, *32*, L12703, doi:10.1029/2005GL023209.

Grist, J. P., and S. A. Josey (2003), Inverse analysis adjustment of the SOC air-sea flux climatology using ocean heat transport constraints, *J. Clim.*, *16*, 3274–3295, doi:10.1175/1520-0442(2003)016<3274:IAAOTS>2.0.CO;2.

Hernández-Guerra, A., T. M. Joyce, E. Fraile-Nuez, and P. Vélez-Belchí (2010), Using Argo data to investigate the meriodional overturning circulation in the North Atlantic, *Deep Sea Res., Part I*, *57*, 29–36, doi:10.1016/j.dsr.2009.10.003.

Hobbs, W. R., and M. N. Raphael (2010), Characterizing the zonally asymmetric component of the SH circulation, *Clim. Dyn.*, *35*, 859–873, doi:10.1007/s00382-009-0663-z.

Hsiung, J. (1985), Estimates of global oceanic meridional heat transport, *J. Phys. Oceanogr.*, *15*, 1405–1413, doi:10.1175/1520-0485(1985)015<1405:EOGOMH>2.0.CO;2.

Huss, M., R. Hock, A. Bauder, and M. Funk (2010), 100-year mass changes in the Swiss Alps linked to the Atlantic Multidecadal Oscillation, *Geophys. Res. Lett.*, *37*, L10501, doi:10.1029/2010GL042616.

Johns, W. E., et al. (2011), Continuous, array-based estimates of Atlantic Ocean heat transport at 26.5°N, *J. Clim.*, *24*, 2429–2449, doi:10.1175/2010JCLI3997.1.

Kanamitsu, M., W. Ebisuzaki, J. Woollen, S.-K. Yang, J. J. Hnilo, M. Fiorino, and G. L. Potter (2002), NCEP-DOE AMIP-II Reanalysis (R-2), *Bull. Am. Meteorol. Soc.*, *83*(11), 1631–1643, doi:10.1175/BAMS-83-11-1631.

Kanzow, T., et al. (2010), Seasonal variability of the Atlantic meridional overturning circulation at 26.5°N, *J. Clim.*, *23*, 5678–5698, doi:10.1175/2010JCLI3389.1.

Kerr, R. A. (2000), A North Atlantic pacemaker for the centuries, *Science*, *288*, 1984–1985, doi:10.1126/science.288.5473.1984.

Knight, J. R., R. J. Allan, C. K. Folland, M. Vellinga, and M. E. Mann (2005), A signature of persistent natural circulation cycles in observed climate, *Geophys. Res. Lett.*, *32*, L20708, doi:10.1029/2005GL024233.

Koltermann, K. P., A. V. Sokov, V. P. Tereschenkov, S. A. Dobroliubov, K. Lorbache, and K. Sy (1999), Decadal changes in the thermohaline circulation of the North Atlantic, *Deep Sea Res., Part II*, *46*, 109–138, doi:10.1016/S0967-0645(98)00115-5.

Lentz, S. J. (2008), Observations and a model of the mean circulation over the Middle Atlantic Bight continental shelf, *J. Phys. Oceanogr.*, *38*, 1203–1221, doi:10.1175/2007JPO3768.1.

Locarnini, R. A., A. V. Mishonov, J. I. Antonov, T. P. Boyer, H. E. Garcia, O. K. Baranova, M. M. Zweng, and D. R. Johnson (2010), *World Ocean Atlas 2009*, vol. 1, *Temperature*, edited by S. Levitus, 184 pp., U.S. Gov. Print. Off., Washington, D. C.

Lozier, M. S., V. Roussenov, M. C. S. Reed, and R. G. Williams (2010), Opposing decadal changes for the North Atlantic meridional overturning circulation, *Nat. Geosci.*, *3*, 728–734, doi:10.1038/ngeo947.

Lumpkin, R., K. G. Speer, and K. P. Koltermann (2008), Transport across 48°N in the Atlantic Ocean, *J. Phys. Oceanogr.*, *38*, 733–752, doi:10.1175/2007JPO3636.1.

McDonagh, E. L., P. McLeod, B. A. King, and H. L. Bryden (2010), Circulation, heat and freshwater transport at 36°N in the Atlantic, *J. Phys. Oceanogr.*, *40*, 2661–2678, doi:10.1175/2010JPO4176.1.

Menemenlis, D., I. Fukumori, and T. Lee (2005a), Using Green's functions to calibrate an ocean general circulation model, *Mon. Weather Rev.*, *133*, 1224–1240, doi:10.1175/MWR2912.1.

Menemenlis, D., et al. (2005b), NASA supercomputer improves prospects for ocean climate research, *Eos Trans. AGU*, *86*(9), 89, 96, doi:10.1029/2005EO090002.

Peña-Molino, B., and T. M. Joyce (2008), Variability in the slope water and its relation to the Gulf Stream path, *Geophys. Res. Lett.*, *35*, L03606, doi:10.1029/2007GL032183.

Reynolds, R. W., N. A. Rayner, T. M. Smith, D. C. Stokes, and W. Wang (2002), An improved in situ and satellite SST analysis for climate, *J. Clim.*, *15*(13), 1609–1625, doi:10.1175/1520-0442(2002)015<1609:AIISAS>2.0.CO;2.

Rintoul, S. R., and C. Wunsch (1991), Mass, heat, oxygen and nutrient fluxes and bugets in the North Atlantic Ocean, *Deep Sea Res.*, *38*(S1), S355–S377.

Roemmich, D., and C. Wunsch (1985), Two transatlantic sections: Meridional circulation and heat flux in the subtropical North Atlantic Ocean, *Deep Sea Res.*, *32*(6), 619–664, doi:10.1016/0198-0149(85)90070-6.

Rowell, D. P., C. K. Folland, K. Maskell, and M. N. Ward (1995), Variability of summer rainfall over tropical North-Africa (1906–92): Observations and modeling, *Q. J. R. Meteorol. Soc.*, *121*, 669–704.

Sato, O. T., and T. Rossby (2000), Seasonal and low-frequency variability of the meridional heat flux at 36°N in the North Atlantic, *J. Phys. Oceanogr.*, *30*, 606–621, doi:10.1175/1520-0485(2000)030<0606:SALFVO>2.0.CO;2.

Sutton, R. T., and D. L. R. Hodson (2005), Atlantic Ocean forcing of North American and European summer climate, *Science*, *309*, 115–118, doi:10.1126/science.1109496.

Talley, L. D. (2003), Shallow, intermediate and deep overturning components of the global heat budget, *J. Phys. Oceanogr.*, *33*(3), 530–560, doi:10.1175/1520-0485(2003)033<0530:SIADOC>2.0.CO;2.

Trenberth, K. E., and J. M. Caron (2001), Estimates of meridional atmospheric and ocean heat transports, *J. Clim.*, *14*, 3433–3443, doi:10.1175/1520-0442(2001)014<3433:EOMAAO>2.0.CO;2.

Volkov, D. L., T. Lee, and L.-L. Fu (2008), Eddy-induced meridional heat transport in the ocean, *Geophys. Res. Lett.*, *35*, L20601, doi:10.1029/2008GL035490.

Weaver, A. J., M. Eby, M. Kienast, and O. A. Saenko (2007), Response of the Atlantic meridional overturning circulation to increasing CO_2: Sensitivity to mean climate state, *Geophys. Res. Lett.*, *34*, L05708, doi:10.1029/2006GL028756.

Willis, J. K. (2010), Can in situ floats and satellite altimeters detect long-term changes in Atlantic Ocean overturning?, *Geophys. Res. Lett.*, *37*, L06602, doi:10.1029/2010GL042372.

Willis, J. K., and L.-L. Fu (2008), Combining altimeter and subsurface float data to estimate the time-averaged circulation in the upper ocean, *J. Geophys. Res.*, *113*, C12017, doi:10.1029/2007JC004690.

Willis, J. K., D. Roemmich, and B. Cornuelle (2003), Combining altimetric height with broadscale profile data to estimate steric height, heat storage, subsurface temperature, and sea-surface temperature variability, *J. Geophys. Res.*, *108*(C9), 3292, doi:10.1029/2002JC001755.

Woodgate, R. A., K. Aagaard, and T. J. Weingartner (2006), Interannual changes in the Bering Strait fluxes of volume, heat and freshwater between 1991 and 2004, *Geophys. Res. Lett.*, *33*, L15609, doi:10.1029/2006GL026931.

Zhang, R. (2010), Latitudinal dependence of Atlantic meridional overturning circulation (AMOC) variations, *Geophys. Res. Lett.*, *37*, L16703, doi:10.1029/2010GL044474.

Zhang, R., S. M. Kang, and I. M. Held (2010), Sensitivity of climate change induced by the weakening of the Atlantic meridional overturning circulation to cloud feedback, *J. Clim.*, *23*, 378–389, doi:0.1175/2009JCLI3118.1.

Zheng, Y., and B. S. Giese (2009), Ocean heat transport in Simple Ocean Data Assimilation: Structure and mechanisms, *J. Geophys. Res.*, *114*, C11009, doi:10.1029/2008JC005190.

W. R. Hobbs and J. K. Willis, NASA Jet Propulsion Laboratory, California Institute of Technology, 4800 Oak Grove Dr., M/S 300–323, Pasadena, CA 91109, USA. (william.r.hobbs@jpl.nasa.gov)